


## Original article

# Interfacial dynamics with soluble surfactants: A phase-field two-phase flow model with variable densities

Guangpu Zhu<sup>1,2</sup>, Aifen Li<sup>1\*</sup>

<sup>1</sup>Research Center of Multiphase Flow in Porous Media, School of Petroleum Engineering, China University of Petroleum (East China), Qingdao 266580, P. R. China

<sup>2</sup>Department of Mechanical Engineering, Johns Hopkins University, Baltimore 21218, USA

### Keywords:

Interfacial dynamics  
phase-field modeling  
surfactant  
two-phase flows  
Navier-Stokes

### Cited as:

Zhu, G., Li, A. Interfacial dynamics with soluble surfactants: A phase-field two-phase flow model with variable densities. *Advances in Geo-Energy Research*, 2020, 4(1): 86-98, doi: 10.26804/ager.2020.01.08.

### Abstract:

In this work, we present a hydrodynamics coupled phase-field surfactant model with variable densities. Two scalar auxiliary variables are introduced to transform the original free energy functional into an equivalent form, and then a new thermodynamically consistent model can be obtained. In this model, evolutions of two phase-field variables are described by two Cahn-Hilliard-type equations, and the fluid flow is dominated by incompressible Navier-Stokes equation. The finite difference method on staggered grid is used to solve the above model. Then a classical droplet rising case and a droplet merging case are used to validate our model. Finally, we study the effect of surfactants on droplet deformation and merging. A more prolate profile of droplet is observed under a higher surfactant bulk concentration, which verifies the effect of surfactant in reducing the interfacial tension. Increases in surface Péclet number and initial surfactant bulk concentration can enhance the non-uniformity of surfactant distribution around the interface, which will arise the Marangoni force. The Marangoni force acts as an additional repulsive force to delay the droplet merging.

## 1. Introduction

Surfactants, interface active agents, are known to lower the interfacial tension and allow for the formation of emulsion (Khatri and Tornberg, 2014; Yang, 2018). Commonly-used surfactants are amphiphilic compounds, meaning they contain both hydrophilic heads and hydrophobic tails (Liu and Zhang, 2010; Khatri and Tornberg, 2014). This special molecular composition enables surfactants to selectively absorb on fluid interfaces. Surfactants play a crucial role in everyday life and many industrial processes (Liu and Zhang, 2010), such as the cleanser essence, the crude oil recovery and pharmaceutical materials, thus having an understanding of their behavior is a necessity. Numerical simulation is taking an increasingly significant position in investigating interfacial phenomena, as it can provide easier access to some quantities such as surfactant concentration, pressure and velocity, which are difficult to measure experimentally (Liu et al., 2018; Yang et al., 2019). However, the computational modeling of interfacial dynamics with surfactants remains a challenging task.

Numerical methods to simulate the multiphase system

with surfactants based on the Navier-Stokes equation (Zhang et al., 2019) can be roughly divided into two categories: sharp interface models and the phase-field model (Wang et al., 2019). Commonly-used sharp interface models include the level set method (Xu et al., 2006, 2012), the volume of fluid (VOF) method (James and Lowengrub, 2004; Alke and Bothe, 2009) and the front tracking method (Muradoglu and Tryggvason, 2008). Although sharp interface models have made great progresses in simulating interfacial flows with surfactants, they still suffer from several drawbacks, such as unphysical re-initialization processes in the level set method and complex interface reconstruction processes in the VOF method. The phase-field model shows great advantages in investigating interfacial phenomena and it has been extensively used with many successes (Shen and Yang, 2015; Van der Sman, 2016; Kou et al., 2018; Kou and Sun, 2018a, 2018b). This method introduces a phase-field variable to distinguish two pure phases, and the interface is treated as a thin layer, inside which the phase-field variable varies continuously (Yue et al., 2004; Chen et al., 2009; Zhu et al., 2017; Kou and



\*Corresponding author.

E-mail address: zhugupc@gmail.com (G. Zhu); aifenli123@163.com (A. Li).

2207-9963 © The Author(s) 2020.

Received February 23, 2020; revised March 7, 2020; accepted March 7, 2020; available online March 9, 2020.

Sun, 2018a). Unlike shape interface models, the phase-field model does not need to track the interface explicitly, and the interface can be implicitly and automatically captured by the evolution of phase-field variable. Therefore, the computations and analysis of the phase-field model are much easier than other models (Xu et al., 2018; Zhu et al., 2019a; Wang et al., 2020).

The phase-field model was first used to study the dynamics of phase separation with surfactants by Laradji et al. (1992). Two phase-field variables were introduced to represent volume fractions of fluids and surfactant concentration, respectively. The original Ginzburg-Landau potential was modified by introducing some additional energy terms to account for the effect of surfactants. Since then, a variety of phase-field surfactant models have been proposed (Komura and Kodama, 1997; Fonseca et al., 2007) and reviews of these models can refer to (Li and Kim, 2012; Van der Sman and Meinders, 2016; Yang and Ju, 2017; Zhu et al., 2018). Here we only highlight two representative works. Van der Sman and Van der Graaf (2006) introduced the logarithmic Flory-Huggins potential to restrict the range of surfactant concentration. A nonlinear coupling surface energy potential was used to attract surfactants onto the fluid interface. An enthalpic term was also adopted to stabilize the phase-field model and control the surfactant solubility in the bulk phases. Engblom et al. (2013) analyzed the well-posedness of the phase-field surfactant model proposed by Van der Sman and Van der Graaf (2006), and provided strong evidence that the model was mathematically ill-posed for a large set of physically relevant parameters. They made critical modifications to the model and substantially increased the domain of validity. Their model can describe realistic adsorption isotherms, e.g., Langmuir isotherm, in thermodynamic equilibrium. In this study, we will use this modified free energy functional to describe a binary fluid-surfactant system.

We can directly obtain chemical potentials through variational derivatives of the free energy functional with respect to two phase-field variables. Two Cahn-Hilliard-type equations can be adopted to describe the evolutions of two phase-field variables (Liu et al., 2018; Zhu et al., 2019c). The hydrodynamics coupled phase-field surfactant model can be obtained if two Cahn-Hilliard-type equations are further coupled to the Navier-Stokes equation. This model allows us to investigate the interfacial dynamics with soluble surfactants. However, nonlinear terms in chemical potentials, arising from the double well potential and Flory-Huggins potential, will bring great difficulties to the construction of numerical schemes and solution of the whole governing system (Zhu et al., 2019b). A strategy is needed to transform the nonlinear potentials in the free energy functional, then we can get a new model, which allows us to design efficient schemes to solve the whole governing system. In this study, we use the scalar auxiliary variable (SAV) approach (Kou et al., 2018; Shen et al., 2018) to transform the free energy functional into an equivalent form. Then a new governing system is obtained by using the variational approach. In particular, two phases with variable densities are considered. Using the new model, we investigate the effect of surfactants on the interfacial flow.

The rest of this paper is organized as follows. In section

2, we present a hydrodynamics coupled phase-field surfactant model with variable densities. Interfacial dynamics with soluble surfactants are investigated in section 3 and the paper is finally concluded in section 4.

## 2. Governing equation

In this section, we consider a typical dimensionless phase-field surfactant model in (Engblom et al., 2013) for a two-phase system with soluble surfactants

$$E_f(\mathbf{u}, \phi, \psi) = \int \left( \frac{Cn^2}{4} |\nabla \phi|^2 + F(\phi) + PiG(\psi) \right) d\Omega + \int (F_s(\phi, \psi) + F_b(\phi, \psi)) d\Omega \quad (1)$$

where two phase-field variables are used in the free energy functional. The first phase-field variable  $\phi$  is used to distinguish two phases,

$$\phi(x, t) = \begin{cases} -1, & \text{fluid I} \\ 1, & \text{fluid II} \end{cases} \quad (2)$$

and it varies continuously across the interface between -1 and 1. The other phase-field variable  $\psi$  is used to represent the surfactant concentration. The parameter  $Cn$  determines the interfacial thickness and  $Pi$  is a time-dependent parameter. The first two terms in Eq. (1) is the Ginzburg-Landau-type energy potential. The square gradient term contributes to the two-phase mixing, while the polynomial part  $F(\phi) = (\phi^2 - 1)^2/4$ , the double well potential, promotes the two-phase separation. The competition between the two terms creates a diffuse interface. The third term  $G(\psi) = \psi \ln \psi + (1 - \psi) \ln(1 - \psi)$  in Eq. (1) is the logarithmic Flory-Huggins potential, and it controls the entropy of mixing soluble surfactants with the bulk phases. The first term  $\psi \ln \psi$  in  $G(\psi)$  models the ideal mixing of surfactants in the bulk phases and guarantees the value of  $\psi$  to be positive, and the second term  $(1 - \psi) \ln(1 - \psi)$  restricts  $\psi < 1$ . The special molecular composition of surfactants enables them to selectively absorb on the fluid interface. A surface energy potential  $F_s = \psi(\phi^2 - 1)^2/4$  is adopted in the free energy functional to account for the high surfactant concentration around the interface. Lastly, the nonlinear coupling term  $F_b = \psi\phi^2/(4Ex)$  in Eq. (1) plays an important role in penalizing free surfactants in the bulk phases and stabilizing the phase-field model. In contrast to the surface energy potential  $F_s$ ,  $F_b$  is inactive at the fluid interface where  $\phi \approx 0$ . However, to some extent,  $F_s$  and  $F_b$  are complementary:  $F_s$  locally attracts surfactants to the fluid interface while  $F_b$  globally counteracts the occurrence of free surfactants. We can directly obtain chemical potentials using the variational approach from the free energy functional (Eq. (1)), but these chemical potentials, arising from the nonlinear double well potential and Flory potential, will bring great difficulties to the construction of numerical schemes and solution of the whole governing system. To solve this problem, a SAV approach is used to transform the free energy functional into a new form, then we can obtain a new phase-field surfactant model for two-phase flow with variable densities. The new model allows

us to develop efficient schemes to investigate the interfacial dynamics with soluble surfactants.

Although both the double well potential  $F(\phi)$  and the Flory-Huggins potential  $G(\psi)$  are bounded from below, the latter is not always positive in the whole domain. We add a zero term  $PiB - PiB$  to the free energy functional (Eq. (1)), and rewrite it into

$$E_f(\phi, \psi) = \int \left( \frac{Cn^2}{4} |\nabla \phi|^2 + Pi(G(\psi) + B) \right) d\Omega + \int \left( F(\phi) + \frac{\psi \phi^2}{4Ex} - \frac{\psi(\phi^2 - 1)^2}{4} \right) d\Omega - PiB|\Omega| \quad (3)$$

where the positive constant  $B$  ensures  $G(\psi) + B > 0$ , and  $B = 1$  is adopted in this study. Note that the free energy is not changed due to the introduction of the zero term  $PiB - PiB$ . We now use the SAV approach (Shen et al., 2018; Zhu et al., 2018) to transform the free energy functional into a new form. The SAV approach was first proposed to construct numerical schemes for the Cahn-Hilliard equation, and the developed scheme is usually energy stable and efficient. Since then the SAV approach has been applied to a large class of gradient flows, because it does not restrict to specific forms of nonlinear parts in the free energy functional (Shen et al., 2019). The idea of the SAV approach is quite simple but quite different from the traditional approach. For example, it does not require the second derivative of  $F(\phi)$  to be bounded as the stabilization approach. Through a simple substitution of scalar auxiliary variables, the nonlinear parts are transformed into quadratic forms of new scalar variables. More precisely, we define two scalar variables

$$U = \sqrt{E_u(\phi)}, \quad V = \sqrt{E_v(\psi)} \quad (4)$$

where

$$E_u(\phi) = \int F(\phi) d\Omega, \quad E_v(\psi) = \int (G(\psi) + B) d\Omega \quad (5)$$

In turn, the free energy functional can be transformed into an equivalent form

$$E_f(\phi, \psi, U, V) = \int \left( \frac{We}{2} \rho |\mathbf{u}|^2 + \frac{Cn^2}{4} |\nabla \phi|^2 \right) d\Omega + \int \left( \frac{\psi \phi^2}{4Ex} - \frac{\psi(\phi^2 - 1)^2}{4} \right) d\Omega + U^2 + PiV^2 - PiB|\Omega| \quad (6)$$

Through the functional derivatives of  $E_f$  with respect to phase-field variables  $\phi$  and  $\psi$  we can obtain chemical potentials  $w_\phi$  and  $w_\psi$

$$w_\phi = -\frac{Cn^2}{2} \Delta \phi + \frac{U}{\sqrt{E_u(\phi)}} F'(\phi) + \frac{\psi \phi}{2Ex} - \psi \phi W$$

$$U_t = \frac{1}{2\sqrt{E_u(\phi)}} \int F'(\phi) \phi_t d\Omega \quad (7)$$

$$w_\psi = \frac{VPi}{\sqrt{E_v(\psi)}} G'(\psi) + \frac{\phi^2}{4Ex} - \frac{W^2}{4}$$

$$V_t = \frac{1}{2\sqrt{E_v(\psi)}} \int G'(\psi) \psi_t d\Omega \quad (8)$$

Note that  $\phi^2 - 1$  are denoted as  $W$  in Eqs. (7) and (8). These two equations allow us to treat nonlinear potentials semi-explicitly when we construct time-marching schemes.

Evolutions of phase-field variables  $\phi$  and  $\psi$  can be described by the conserved Cahn-Hilliard-type equations (Engblom et al., 2013),

$$\phi_t + \nabla \cdot (\mathbf{u} \phi) = \frac{1}{Pe_\phi} \Delta w_\phi \quad (9)$$

$$\psi_t + \nabla \cdot (\mathbf{u} \psi) = \frac{1}{Pe_\psi} \nabla \cdot M_\psi \nabla w_\psi \quad (10)$$

where  $Pe_\phi$  and  $Pe_\psi$  are Péclet numbers. A degenerate mobility  $M_\psi = \psi(1 - \psi)$ , which vanishes at the extreme points  $\psi = 0$  and  $\psi = 1$  adopted to combine with the logarithmic chemical potential Eqs. 7 – 10, are coupled to the Navier-Stokes equation in the form (Engblom et al., 2013; Shen and Yang, 2015)

$$\rho \mathbf{u}_t + \rho \mathbf{u} \cdot \nabla \mathbf{u} + \mathbf{J} \cdot \nabla \mathbf{u} - \frac{\nabla \cdot \eta D(\mathbf{u})}{Re} + \nabla p + \frac{(\phi \nabla w_\phi + \psi \nabla w_\psi)}{Re Ca Cn} = 0 \quad (11)$$

$$\nabla \cdot \mathbf{u} = 0 \quad (12)$$

where  $D(\mathbf{u}) = \nabla \mathbf{u} + \nabla^T \mathbf{u}$  and  $\mathbf{J} = (\lambda_\rho - 1) \nabla w_\phi / 2Pe_\phi$ .  $\mathbf{u}$  is the velocity field,  $p$  is the pressure,  $Re$  is the Reynolds number and  $Ca$  is the Capillary number. We usually assume the density  $\rho$  and viscosity  $\eta$  have the following linear relations (Yuan et al., 2019),

$$\rho = \frac{1 - \lambda_\rho}{2} \phi + \frac{1 + \lambda_\rho}{2}, \quad \eta = \frac{1 - \lambda_\eta}{2} \phi + \frac{1 + \lambda_\eta}{2} \quad (13)$$

where  $\lambda_\rho$  and  $\lambda_\eta$  are density and viscosity ratios, respectively.

In particular, if we consider a body force, e.g., the gravitational force, the dimensionless momentum equation read

$$\rho \mathbf{u}_t + \rho \mathbf{u} \cdot \nabla \mathbf{u} + \mathbf{J} \cdot \nabla \mathbf{u} - \frac{\nabla \cdot \eta D(\mathbf{u})}{Re} + \nabla p + \frac{(\phi \nabla w_\phi + \psi \nabla w_\psi)}{Bo Cn} - \rho \mathbf{g} = 0 \quad (14)$$

where  $Bo = Re Ca$  is the Bond number, and  $\mathbf{g}$  is the unit vector denoting the direction of body force.

Periodic boundary conditions or the following boundary conditions

$$\partial_n \phi^{n+1} = \nabla w_\phi^{n+1} \cdot \mathbf{n} = \nabla w_\psi^{n+1} \cdot \mathbf{n}$$

$$= \nabla p^{n+1} \cdot \mathbf{n} = \mathbf{u} = 0, \quad \text{on } \Gamma \quad (15)$$

can be used to close the above governing system. Here denotes boundaries of the domain.

The total energy  $E_{tot}$  of the hydrodynamic system Eqs. 7 - 12 is the sum of kinetic energy  $E_k$  and free energy  $E_f$

$$E_{tot} = \int \left( \frac{We}{2} \rho |\mathbf{u}|^2 + \frac{Cn^2}{4} |\nabla \phi|^2 + \frac{\psi \phi^2}{4Ex} - \frac{\psi(\phi^2 - 1)^2}{4} \right) d\Omega + U^2 + PiV^2 - PiB|\Omega| \quad (16)$$

where  $We = ReCaCn$ , and we can easily derive the following energy dissipation law

$$\begin{aligned} \frac{d}{dt} E_{tot} = & -\frac{1}{Pe_\phi} \int |\nabla w_\phi|^2 d\Omega - \frac{1}{Pe_\psi} \int |\sqrt{M_\psi} \nabla w_\psi|^2 d\Omega \\ & - \frac{CaCn}{2} \int |\sqrt{\eta} D(\mathbf{u})|^2 d\Omega \leq 0 \end{aligned} \quad (17)$$

The equation (Eq. 16) indicates that the governing Eqs. 7 – 12 is thermodynamically consistent.

An efficient energy-stable time-marching scheme can be easily constructed for the above governing equation, and details can refer to Zhu et al. (2019b); Zhu et al. (2020). Note that the current work is the extension of matched density case in (Zhu et al., 2019b). The SAV approach used in this study is more accurate and efficient than the IEQ approach used in (Zhu et al., 2019b). Also, the variable density case considered in this study presents new challenges to the development of energy stable time-marching scheme, and we can only construct a nonlinearly coupled scheme for the above governing equation. We use a finite difference method on staggered grids to discretize space. For simplicity, the computational domain is divided into uniform rectangular meshes. The phase-field variables  $\phi$  and  $\psi$  the chemical potentials  $w_\phi$  and  $w_\psi$  the pressure  $p$ , the density  $\rho$  and the viscosity  $\eta$  are defined at cell centers. Velocities in  $x$ ,  $y$  and  $z$  directions are defined at cell face centers.  $U$  and  $V$  are scalar variables. We pay special attention to the discretization of the convection terms in the Cahn-Hilliard and Navier-Stokes equations. A composite high resolution scheme, known as the MINMOD scheme (Li et al., 2015; Moukalled et al., 2016), is used to reduce the undershoot and overshoot around the interface when the density ratio is large. A BICGSTAB method is used to solve the above variables (Yan et al., 2019; Zeng et al., 2019; Sheng et al., 2020). For variable-coefficient equations, matrices for the corresponding constant-coefficient systems are used as preconditioners.

### 3. Results and discussion

In this section, we perform a series of numerical experiments to investigate the interfacial dynamics with soluble surfactants.

#### 3.1 Model validation

The hydrodynamics coupled phase-field model with soluble surfactants in this study can be divided into two sub-models: the hydrodynamics coupled phase-field model with variable densities and the phase-field surfactant model (no hydrodynamics). At first, a classical bubble rising case is to validate the hydrodynamics coupled phase-field model. Then

we use the commercial software - COMSOL to validate the phase-field surfactant model (Comsol, 2012).

The bubble rising process is simulated in a computational domain  $\omega = [0, 1] \times [0, 2]$ . We consider Neumann boundary conditions for all variables except the velocity. The no-slip boundary conditions are imposed on the top and bottom surfaces, and the full slip boundary conditions are applied on the left and right sides of the domain. Note that the full slip boundary condition means that the gradient of vertical velocity component  $v$  is zero in this study. The initial profile of the phase-field variable  $\phi$  is set as

$$\phi(x, y) = -\tanh \left( \frac{\sqrt{(x-0.5)^2 + (y-0.5)^2} - 0.25}{Cn} \right) \quad (18)$$

A grid size of  $200 \times 400$  and time step-size  $\delta t = 2.5 \times 10^{-4}$  are used in our simulation. The Reynolds number  $Re$  and the Bond number are 98.99 and 4, respectively. The Péclet number  $Pe_\phi$  is 10, and the Cahn number  $Cn$  is 0.01. As in (Hysing et al., 2009), we calculate the mass center of bubble  $y_c$  and the rising velocity  $V_c$ ,

$$\begin{aligned} y_c &= \frac{\int_{\phi \geq 0} y \rho d\Omega}{\int_{\phi \geq 0} \rho d\Omega} \\ V_c &= \frac{\int_{\phi \geq 0} y d\Omega}{\int_{\phi \geq 0} 1 d\Omega} \end{aligned} \quad (19)$$

Fig. 1 gives droplet profiles at  $t = 3$ , and Fig. 2 shows evolutions of the mass center and rising velocity. Obviously, our results agree well with the reference solutions from (Hysing et al., 2009).

Now we validate the phase-field surfactant model. The “weak form PDE” module in COMSOL is used to realize the phase-field surfactant model. Note that PDE is an abbreviation of partial differential equation. The computational domain  $\omega$  is set as  $[0, 4] \times [0, 3]$ . Neumann boundary conditions are applied for all variables on boundaries. The initial profile of the phase-field variable  $\phi$  is set as

$$\begin{aligned} \phi(x, y) = & -\tanh \left( \frac{\sqrt{(x-1.18)^2 + (y-1.5)^2} - 0.8}{Cn} \right) \\ & -\tanh \left( \frac{\sqrt{(x-2.82)^2 + (y-1.5)^2} - 0.8}{Cn} \right) + 1 \end{aligned} \quad (20)$$

A grid size of  $300 \times 150$  is used in both COMSOL and our codes. The initial surfactant bulk concentration  $\psi_b$  is  $1 \times 10^{-2}$ , and other important parameters are as follows:

$$Pe_\phi = 10, Pe_\psi = 50, Cn = 0.0283, Ex = 1, \text{ and } Pi = 0.1227$$

Fig. 3 gives the evolution of two droplets and Fig. 4 shows the surfactant concentration along a horizontal line from the

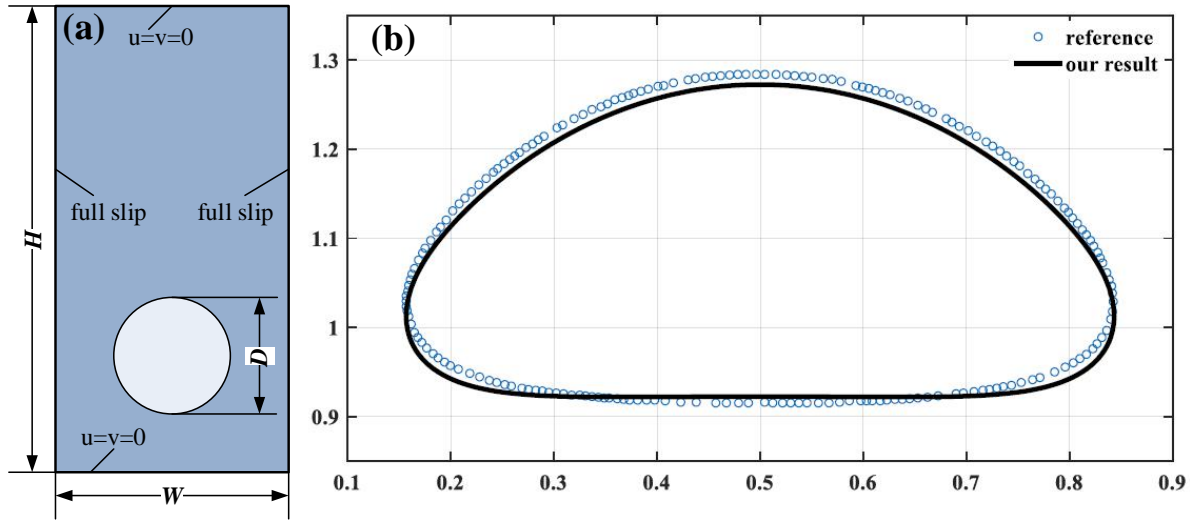


**Fig. 1.** (a) Initial configuration and velocity boundary conditions for the bubble rising case:  $H = 2$ ,  $W = 1$  and  $D = 0.5$ . (b) Droplet profiles ( $\phi = 0$ ) at  $t = 3$ . Black line: our result; blue circle: reference solution.

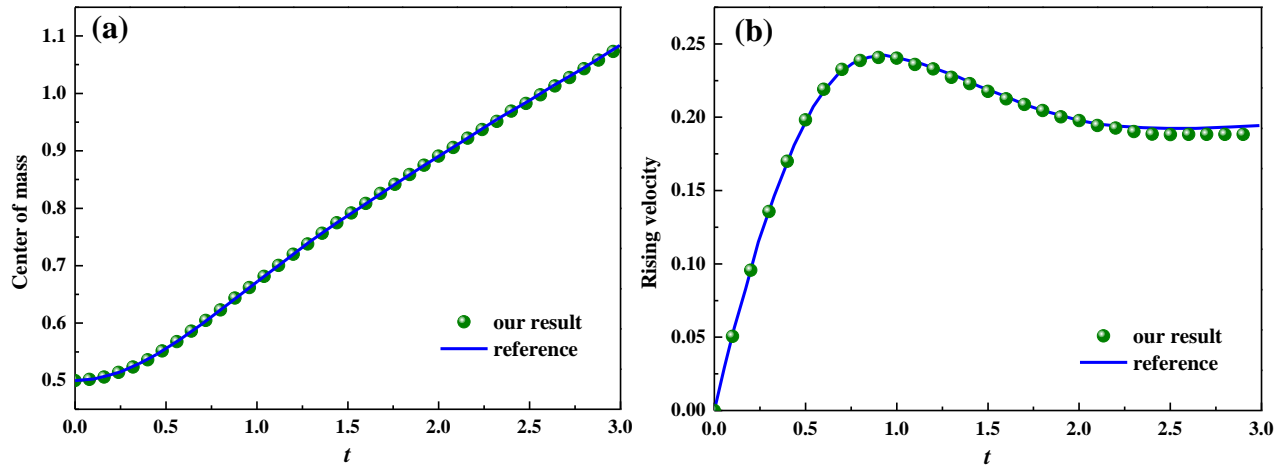


**Fig. 2.** Evolutions of (a) mass center (b) rising velocity of the bubble. Green dot: our results; blue line: reference solutions.

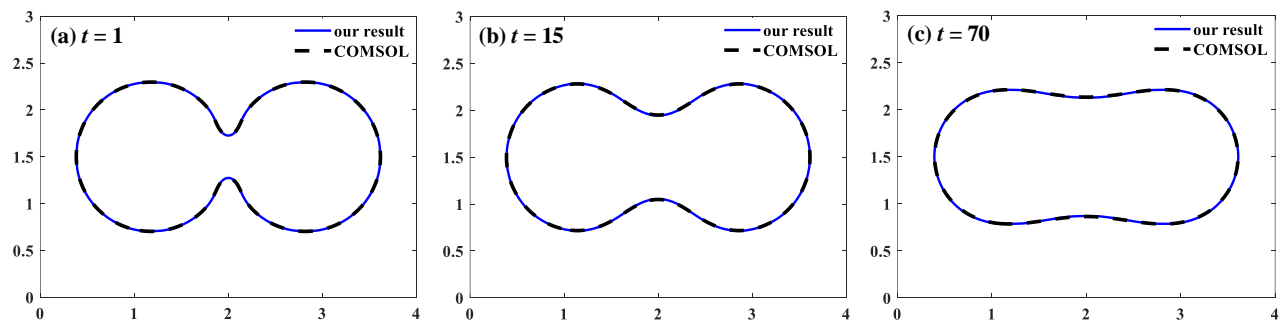


**Fig. 3.** Droplet profiles ( $\phi = 0$ ) at different times. The initial surfactant bulk concentration  $\psi_b = 1 \times 10^{-2}$ . Black dotted line: results obtained by the COMSOL; blue line: our results.

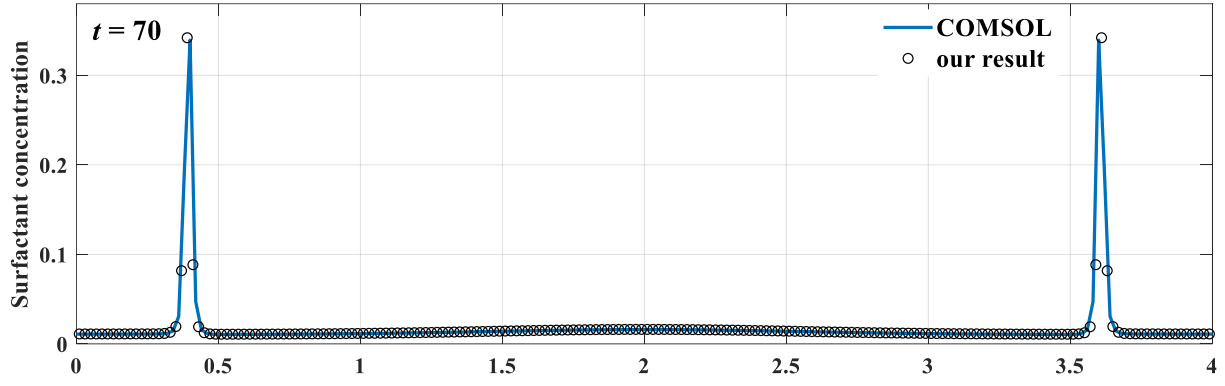


**Fig. 4.** Surfactant concentration along a horizontal line from the point (0, 1.5) to the point (4, 1.5). Blue line: results obtained by COMSOL; black circle: our results.

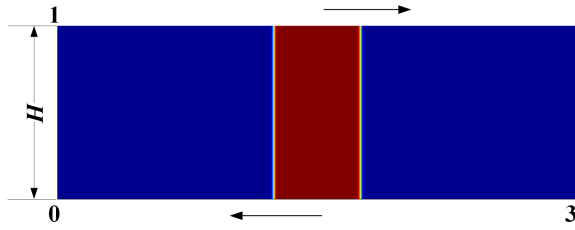


**Fig. 5.** Initial profile of the phase-field variable  $\phi$ .

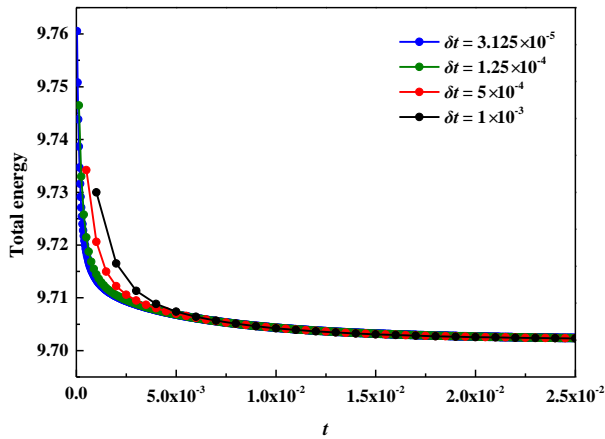


**Fig. 6.** Energy dissipation properties of the proposed scheme.

point (0, 1.5) to the point (4, 1.5). Both of them demonstrate that our results agree well with the results obtained by COMSOL.

### 3.2 Couette flow

In the first test, we simulate the Couette flow in a computational domain  $\Omega = [0, 3] \times [0, 1]$  with periodic boundary conditions (all variables) applied on the left and right sides, as sketched in Fig. 5. We specify the red phase as fluid 1 and the blue phase as fluid 2. Equal but opposite velocities are imposed on the top and bottom walls, respectively. Neumann boundary conditions are applied for phase-field variables, chemical

potentials and pressure, as shown in Eq. (15). Initially, we set the initial surfactant bulk concentration  $\psi_b = 1 \times 10^{-3}$  and the profile of  $\phi$  as

$$\phi_0(x, y) = \tanh\left(\frac{1}{Cn} \left(\frac{L_x}{12} - \left|x - \frac{L_x}{2}\right|\right)\right) \quad (21)$$

Other parameters used in simulations are given below:  $Pe_\phi = 10$ ,  $Pe_\psi = 100$ ,  $Re = 10$ ,  $Ca = 0.1$ ,  $Cn = 0.01$ ,  $Ex = 1$ ,  $Pi = 0.1227$ ,  $\lambda_p = 10$ , and  $\lambda_v = 10$ .

We first study the evolution of the total free energy  $E_{tot}$ . To ensure no input energy from the outside, wall moving velocities  $u_w$  are set to zero. The trend of all four energy curves in Fig. 6 confirms that our schemes are energy stable. Considerable differences between different time step-sizes can also be observed, which mean that the induced numerical errors with large time step-sizes are higher.

Having demonstrated the energy stability, we investigate the effect of surfactants on fluid deformation under a shear flow. A  $480 \times 160$  spatial resolution and time step-size  $2.5 \times 10^{-4}$  are used. We consider three different values ( $1 \times 10^{-6}$ ,  $1.5 \times 10^{-2}$ , and  $5 \times 10^{-2}$ ) in simulations. Fig. 7 gives the evolutions of two phase-field variables  $\phi$  and  $\psi$ . The fluid 1 (red phase) continues to deform until it breaks under a linear shear flow, and surfactants are always adsorbed onto the interface. Note that the surfactant concentration along the fluid interface is non-uniform, and the lowest value appears near walls. However, the surfactant concentration gradient will arise the tangential Marangoni stress (Liu and Zhang, 2010; Liu et al., 2018), which resists the accumulation of surfactants. Fig. 8 shows the profiles of  $\phi$  for three different  $\psi_b$  values. The increase in  $\psi_b$  leads to more obvious deformation, and this can be attributed to a more obvious reduction of surface tension under the larger  $\psi_b$ .

### 3.3 Droplet deformation

We next simulate the droplet deformation under the horizontal body force and a shear flow. We use the same computational domain and settings as the section 4.2. Boundary conditions are same as section 3.2. A circular droplet with the radius of  $r = 0.3$  is initially placed at (1, 0.5). Other simulation



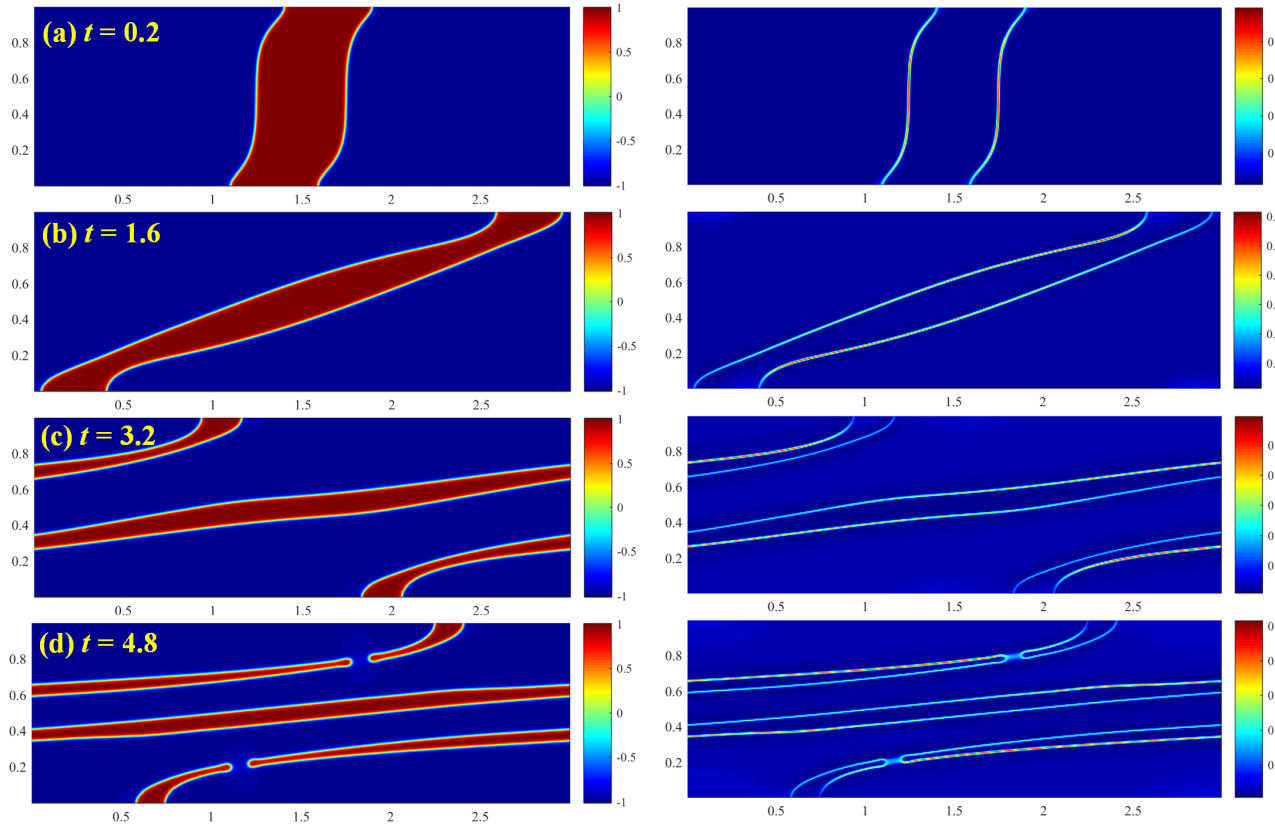


**Fig. 7.** Evolutions of phase-field variables  $\phi$  and  $\psi$ . For each subfigure, the left is the profile of  $\phi$ , and the right is the profile of  $\psi$  ( $\psi_b = 1.5 \times 10^{-2}$ ).

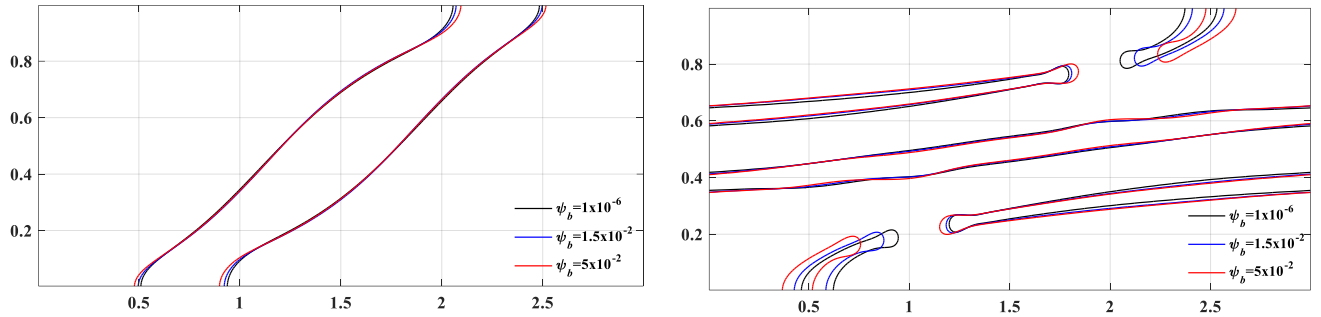


**Fig. 8.** Evolutions of the phase-field variable  $\phi$  in a shear flow at  $t = 1$  (left) and  $t = 5$  (right) (black:  $\psi_b = 1 \times 10^{-6}$ ; blue:  $\psi_b = 1.5 \times 10^{-2}$ ; red:  $\psi_b = 5 \times 10^{-2}$ ).

parameters are listed as follows:  $Pe_\phi = 10$ ,  $Pe_\psi = 100$ ,  $Re = 10$ ,  $Bo = 1$ ,  $Cn = 0.01$ ,  $Ex = 1$ ,  $Pi = 0.1227$ ,  $\lambda_p = 10$ , and  $\lambda_v = 10$ .

Fig. 9 shows the time evolution plots of droplet deformation and surfactant concentration. The droplet continuously deforms and moves forward under the action of the shear flow and the body force. We can divide the whole process into two stages based on the droplet deformation and surfactant migration. At the first stage, the body force has limited effect on the droplet deformation compared with the shear flow. Surfactants gradually migrate toward droplet tips, as shown in Fig. 9(b), resulting in the non-uniformity of interfacial tension along the interface. As we mentioned before, the surfactant concentration gradient induces the Marangoni stress, which

will resist the further migration of surfactants. However, the Marangoni stress is not large enough to balance the effect of shear flow, and surfactants continue to move toward tips. In Fig. 9(c), surfactants are swept into the bulk phases when concentration reaches the maximum at the droplet tips. At the second stage, the body force plays an important role in the droplet deformation and surfactant migration. In Fig. 9(d), surfactants on the tip A are slowly swept towards the ABC segment under the effect of the body force. Surfactants along the ADC segment continuously move to the tips under the combined action of the shear flow and the body force.

Fig. 10 demonstrates the profiles of phase-field variable  $\phi$  at three different  $\psi_b$  value. A more prolate profiles of  $\phi$  is observed for a higher surfactant bulk concentration, which

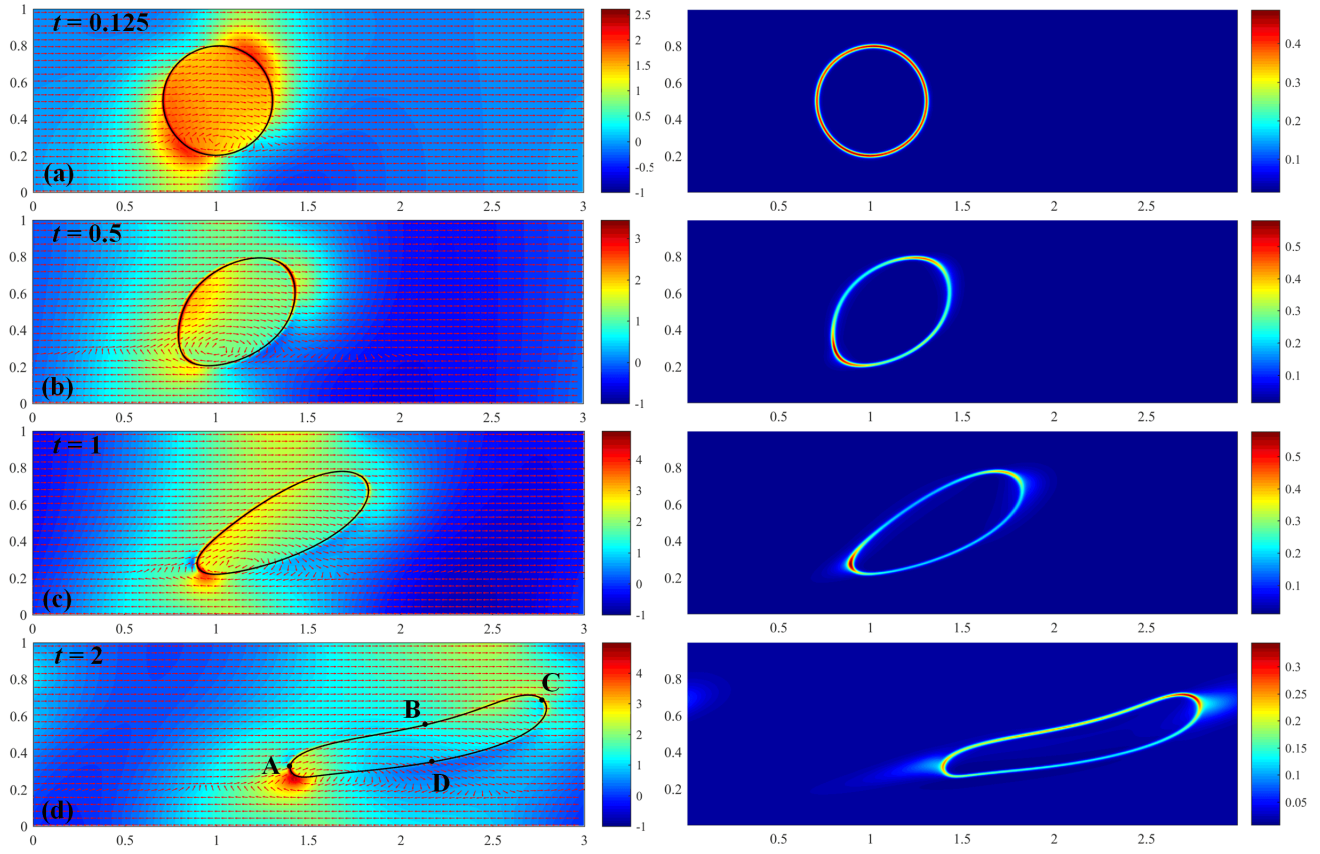


**Fig. 9.** Evolutions of pressure field (background color), quiver plot of velocity  $(u, v)$ , phase-field variables  $\phi$  and  $\psi$ . For each subfigure, the right is the profile of  $\psi$  ( $\psi_b = 1.5 \times 10^{-2}$ ).

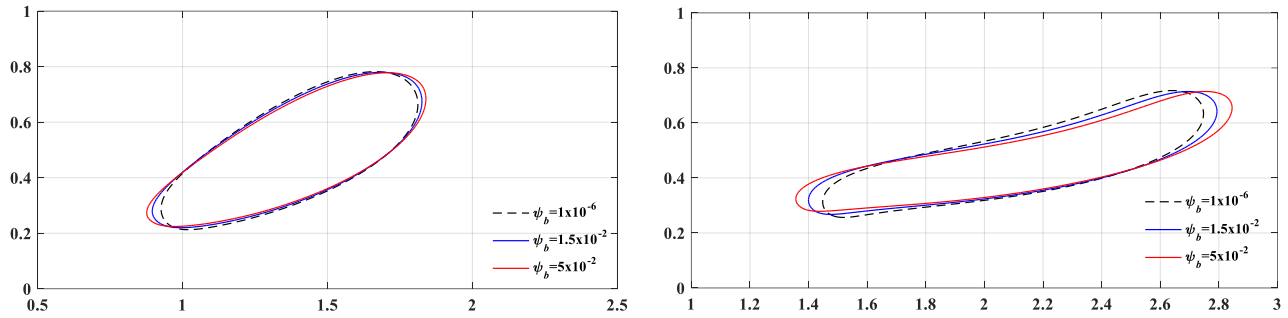


**Fig. 10.** Profiles of phase-field variable  $\phi$  at  $t = 1$  (left) and  $t = 2$  (right) (black dash line:  $\psi_b = 1 \times 10^{-6}$ ; blue solid line:  $\psi_b = 1.5 \times 10^{-2}$ ; red solid line:  $\psi_b = 5 \times 10^{-2}$ ).

confirms the effect of surfactants in reducing the interfacial tension.

We continue to extend our simulations to a three-dimensional (3D) domain  $\Omega = [0, 3] \times [0, 0.8] \times [0, 1]$ . A shear flow is introduced to this system by moving the top and bottom walls with equal but opposite velocities. We also apply a body force along the  $x$  direction. A  $240 \times 64 \times 80$  grid and time step-size  $1 \times 10^{-3}$  are used. Here we list other simulation parameters:  $Pe_\phi = 100$ ,  $Pe_\psi = 20$ ,  $Re = 10$ ,  $Bo = 1$ ,  $Cn = 0.018$ ,  $Ex = 1$ ,  $Pi = 0.1227$ ,  $\lambda_p = 10$ , and  $\lambda_v = 10$ .

Results in Fig. 11 are consistent with the two-dimensional (2D) results in Fig. 9. Again, the profiles of  $\phi$  in Fig. 12 demonstrate that the effect of surfactants in reducing the

interfacial tension.

### 3.4 Two droplets merging

We investigate the merging of droplets (Espath et al., 2016) under the gravitational effect in a closed domain  $\Omega = [0, 1] \times [0, 3]$ . Periodic boundary conditions are applied on top and bottom boundaries. Neumann boundary conditions are applied for phase-field variables, chemical potentials and pressure. Initially, two circular droplets (the red phase) with radius of  $r_1 = 0.25$  and  $r_2 = 0.17$  locate at  $(0.5, 0.45)$  and  $(0.5, 1)$ , respectively. The initial surfactant bulk concentration is  $\psi_b = 1.5 \times 10^{-2}$ . We use a spatial resolution  $160 \times 480$  and time



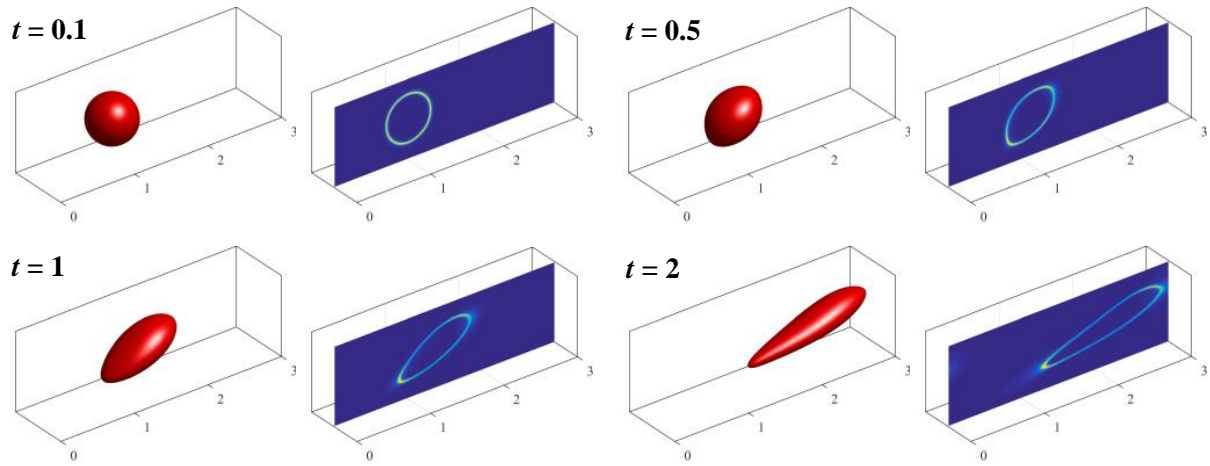


**Fig. 11.** Evolutions of phase-field variables  $\phi$  and  $\psi$ . For each subfigure, the left is the profile of  $\phi$ , and the right is the profile of  $\psi$  ( $\psi_b = 1.5 \times 10^{-2}$ ).

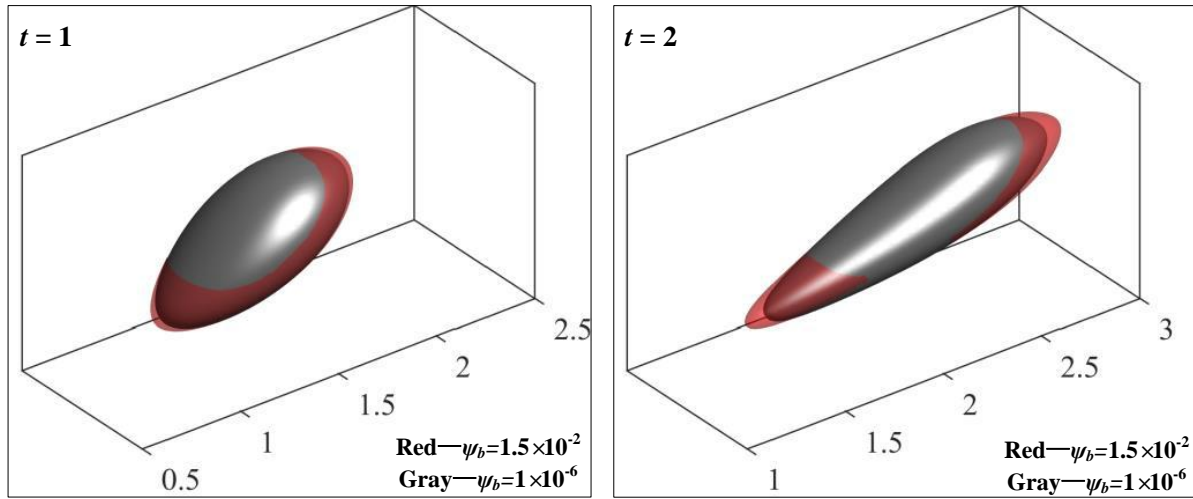


**Fig. 12.** Profiles of phase-field variable  $\phi$  at  $t = 1$  (left) and  $t = 2$  (right) (gray:  $\psi_b = 1 \times 10^{-6}$ ; red:  $\psi_b = 1.5 \times 10^{-2}$ ).

step-size  $\delta t = 2.5 \times 10^{-4}$ . Other parameters are as follows:  $Pe_\phi = 10$ ,  $Pe_\psi = 10$ ,  $Re = 50$ ,  $Bo = 8$ ,  $Cn = 0.01$ ,  $Ex = 1$ ,  $Pi = 0.1227$ ,  $\lambda_p = 8$ , and  $\lambda_v = 10$ .

Fig. 13 shows the time evolution plots of streamlines and profiles of phase-field variables. Two separating droplets with different sizes gradually approach each other and finally merge into one droplet under the gravitational effect. Surfactants are swept towards the bottom of droplets during this process.

The surface Péclet number  $Pe_\psi$  has a clear physical meaning, and it plays an important role on the surfactant distribution along the interface. To study the effect of  $Pe_\psi$  on the surfactant migration and merging of droplets, we consider two different values of  $Pe_\psi$  ( $Pe_\psi = 10$  and  $100$ ) in simulations. The change of surfactant concentration at points A (the top of big droplet,  $\psi_A$ ) and B (the bottom of small droplet,  $\psi_B$ ) are monitored to quantitatively describe the effect of  $Pe_\psi$ . At the point A, the surfactant concentration at  $Pe_\psi = 100$  is obviously lower than that at  $Pe_\psi = 10$ , while the values of  $\psi_B$  present the opposite results, as shown in Fig. 14. We can conclude that the increase in  $Pe_\psi$  can enhance the non-uniformity of surfactant concentration, which will arise the Marangoni

stress. The Marangoni stress acts as an additional repulsive force to prevent the droplet coalescence, which explains the delay of droplet merging at a larger  $Pe_\psi$  in Fig. 15.

To clearly demonstrate the effect of surfactants on the droplet merging,  $Pe_\psi$  is taken as 100, and two different values of  $\psi_b$  are chosen ( $\psi_b = 1 \times 10^{-6}$  and  $1.5 \times 10^{-2}$ ). Fig. 16 indicates that the increase in  $\psi_b$  can also delay the merging of droplets. The Marangoni stress and the enhanced droplet deformation at the low interfacial tension are the main reasons for this phenomenon.

#### 4. Conclusion

In this work, we present a hydrodynamics coupled phase-field surfactant model with variable densities. Two scalar auxiliary variables are introduced to transform the original free energy functional into an equivalent form, and then a new thermodynamically consistent governing system can be obtained. In this model, evolutions of two phase-field variables are determined by two Cahn-Hilliard-type equations, and the fluid flow is dominated by the incompressible Navier-

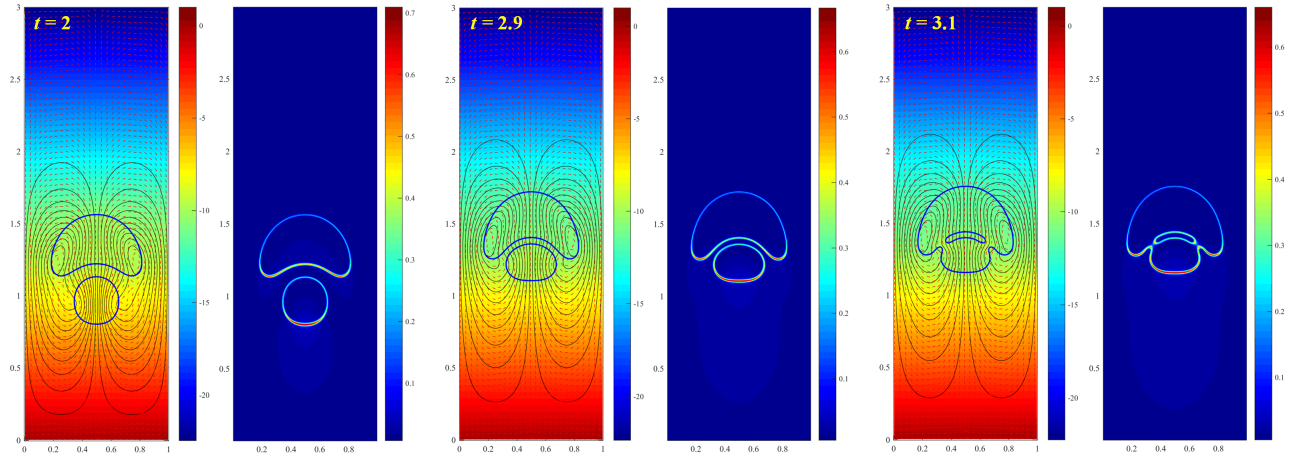


**Fig. 13.** Pressure field (background color), streamlines, contour line of  $\phi = 0$ , quiver plot of velocity ( $u, v$ ) and surfactant concentration. For each subfigure, the right is the surfactant concentration ( $\psi_b = 1.5 \times 10^{-2}$  and  $Pe_\psi = 10$ ).

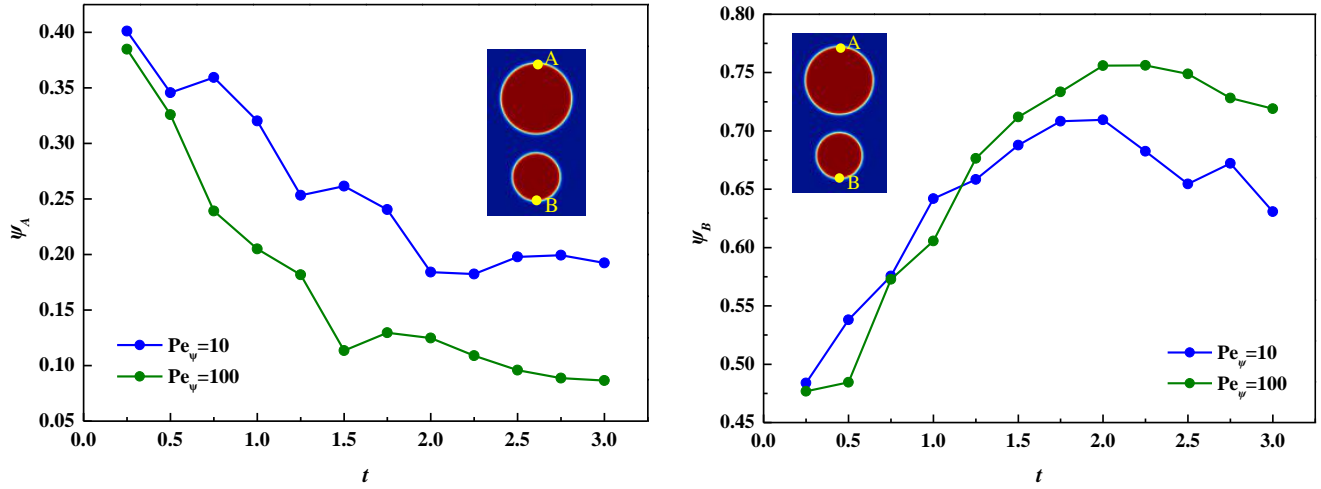


**Fig. 14.** Evolutions of the surfactant concentration at points A and B at various  $Pe_\psi$ .

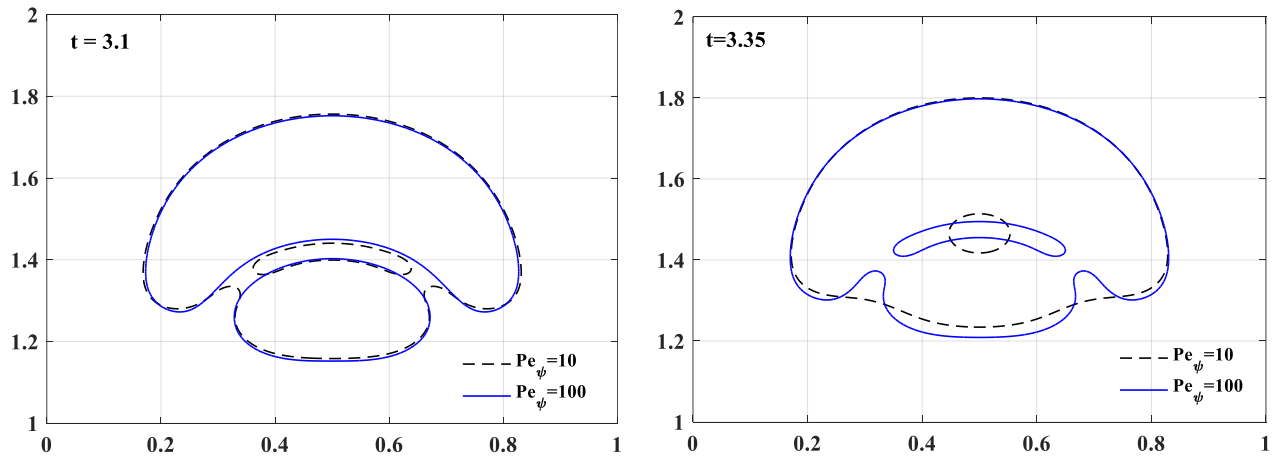


**Fig. 15.** Profiles of phase-field variable  $\phi$  at various  $Pe_\psi$  ( $\psi_b = 1.5 \times 10^{-2}$ ).

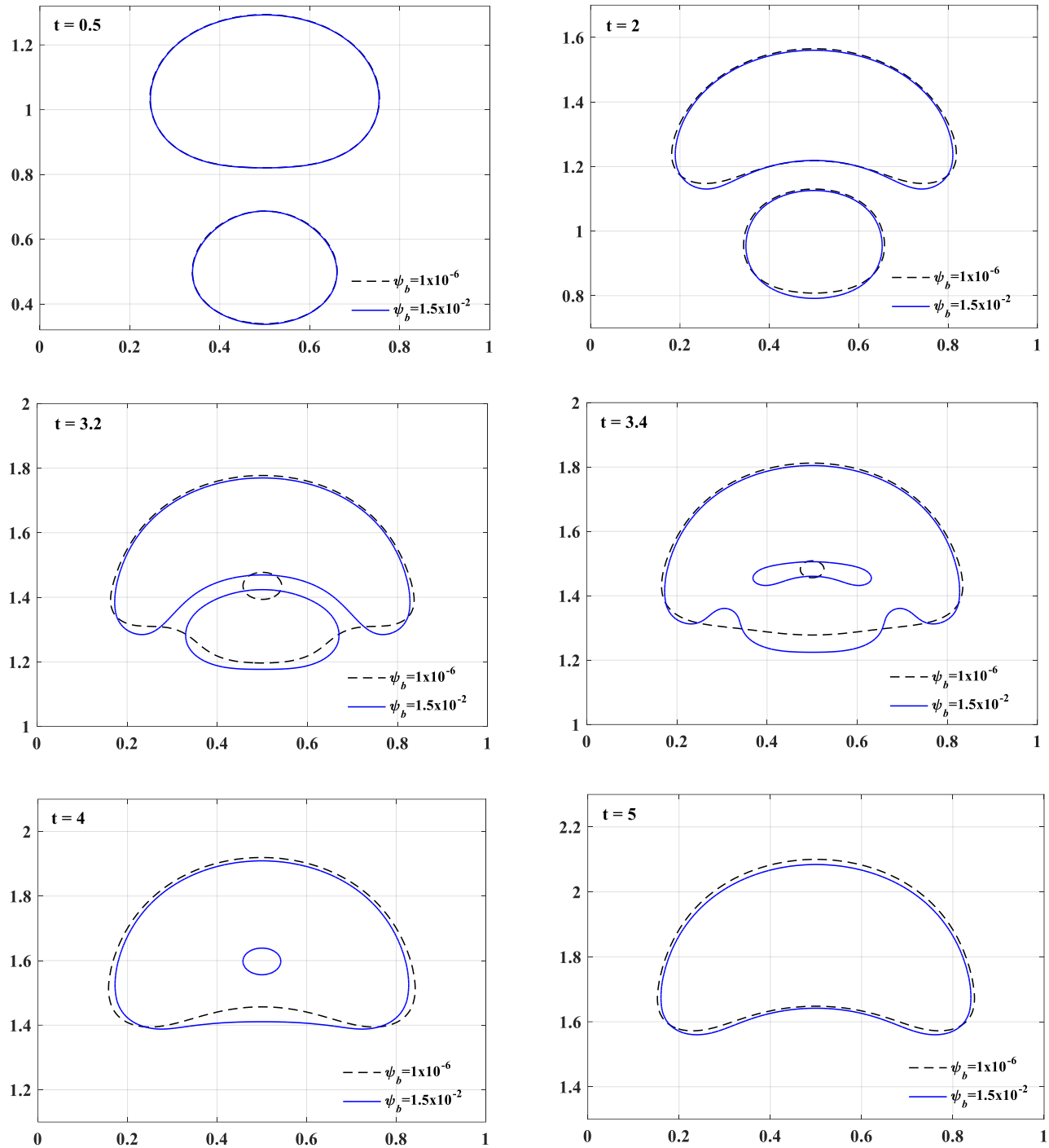


**Fig. 16.** Evolutions of phase-field variable  $\phi$  at different  $\psi_b$  ( $Pe_\psi = 100$ ).

Stokes equation. We also construct some efficient and easy-to-implement schemes to solve the above governing system. In these schemes, nonlinear terms in chemical potentials are treated semi-explicitly, and a splitting method based on pressure stabilization is used to solve the Navier-Stokes equation. Then a classical droplet rising case and a droplet merging case are used to validate our model and schemes. Finally, we study the effect of surfactants on droplet deformation and merging. A more prolate profile of droplet is observed under a higher surfactant bulk concentration, which verifies the effect

of surfactants in reducing the interfacial tension. Increases in surface Péclet number and surfactant bulk concentration can enhance the non-uniformity of surfactant distribution around the interface, which will arise the Marangoni force. The Marangoni force acts as an additional repulsive force to delay the droplet merging.

### Acknowledgement

Authors acknowledge that this work is supported by the

National Natural Science Foundation of China (51804325, 5167428041 and 51774317) and Shandong Provincial Natural Science Foundation (ZR2019JQ21).

## Conflict of interest

The authors declare no competing interest.

**Open Access** This article, published at Ausasia Science and Technology Press on behalf of the Division of Porous Flow, Hubei Province Society of Rock Mechanics and Engineering, is distributed under the terms and conditions of the Creative Commons Attribution (CC BY-NC-ND) license, which permits unrestricted use, distribution, and reproduction in any medium, provided the original work is properly cited.

## References

- Alke, A., Bothe, D. 3D numerical modeling of soluble surfactant at fluidic interfaces based on the volume-of-fluid method. *Fluid Dyn. Mater. Process.* 2009, 5(4): 345-372.
- Chen, C., Tsai, Y.L., Lan, C. Adaptive phase field simulation of dendritic crystal growth in a forced flow: 2D vs 3D morphologies. *Int. J. Heat Mass Transf.* 2009, 52(5-6): 1158-1166.
- Comsol, A.B. COMSOL Multiphysics User's Guide (version 4.3). 2012.
- Engblom, S., Do-Quang, M., Amberg, G., et al. On diffuse interface modeling and simulation of surfactants in two-phase fluid flow. *Commun. Comput. Phys.* 2013, 14(4): 879-915.
- Espath, L.F.R., Sarmiento, A.F., Vignal, P., et al. Energy exchange analysis in droplet dynamics via the Navier-Stokes-Cahn-Hilliard model. *J. Fluid Mech.* 2016, 797: 389-430.
- Fonseca, I., Morini, M., Slastikov, V. Surfactants in foam stability: A phase-field model. *Arch. Ration. Mech. An.* 2007, 183(3): 411-456.
- Hysing, S., Turek, S., Kuzmin, D., et al. Quantitative benchmark computations of twodimensional bubble dynamics. *Int. J. Numer. Meth. Fl.* 2009, 60(11): 1259-1288.
- James, A.J., Lowengrub, J. A surfactant-conserving volume-of-fluid method for interfacial flows with insoluble surfactant. *J. Comput. Phys.* 2004, 201(2): 685-722.
- Khatri, S., Tornberg, A.K. An embedded boundary method for soluble surfactants with interface tracking for two-phase flows. *J. Comput. Phys.* 2014, 256: 768-790.
- Komura, S., Kodama, H. Two-order-parameter model for an oil-water-surfactant system. *Phys. Rev. E* 1997, 55(2): 1722-1727.
- Kou, J., Sun, S. Thermodynamically consistent modeling and simulation of multi-component two-phase flow with partial miscibility. *Comput. Methods Appl. Mech. Eng.* 2018a, 331: 623-649.
- Kou, J., Sun, S. Thermodynamically consistent simulation of nonisothermal diffuse-interface two-phase flow with Peng-Robinson equation of state. *J. Comput. Phys.* 2018b, 371: 581-605.
- Kou, J., Sun, S., Wang, X. Linearly decoupled energy-stable numerical methods for multicomponent two-phase compressible flow. *SIAM J. Numer. Anal.* 2018, 56(6): 3219-3248.
- Laradji, M., Guo, H., Grant, M., et al. The effect of surfactants on the dynamics of phase separation. *J. Phys. Condens. Matter* 1992, 4(32): 6715-6728.
- Li, J., Yu, B., Wang, Y., et al. Study on computational efficiency of composite schemes for convection-diffusion equations using single-grid and multigrid methods. *J. Therm. Sci. Technol.* 2015, 10(1): JTST0009.
- Li, Y., Kim, J. A comparison study of phase-field models for an immiscible binary mixture with surfactant. *Eur. Phys. J. B* 2012, 85(10): 340.
- Liu, H., Ba, Y., Wu, L., et al. A hybrid lattice Boltzmann and finite difference method for droplet dynamics with insoluble surfactants. *J. Fluid Mech.* 2018, 837: 381-412.
- Liu, H., Zhang, Y. Phase-field modeling droplet dynamics with soluble surfactants. *J. Comput. Phys.* 2010, 229(24): 9166-9187.
- Moukalled, F., Mangani, L., Darwish, M. *The Finite Volume Method in Computational Fluid Dynamics: An Advanced Introduction with OpenFOAM and Matlab*. Heidelberg, German, Springer, 2016.
- Muradoglu, M., Tryggvason, G. A front-tracking method for computation of interfacial flows with soluble surfactants. *J. Comput. Phys.* 2008, 227(4): 2238-2262.
- Shen, J., Xu, J., Yang, J. The scalar auxiliary variable (SAV) approach for gradient flows. *J. Comput. Phys.* 2018, 353: 407-416.
- Shen, J., Xu, J., Yang, J. A new class of efficient and robust energy stable schemes for gradient flows. *SIAM Rev.* 2019, 61(3): 474-506.
- Shen, J., Yang, X. Decoupled, energy stable schemes for phase-field models of two-phase incompressible flows. *SIAM J. Numer. Anal.* 2015, 53(1): 279-296.
- Sheng, G., Zhao, H., Su, Y., et al. An analytical model to couple gas storage and transport capacity in organic matter with noncircular pores. *Fuel* 2020, 268: 117288.
- Van der Sman, R.G.M. Phase field simulations of ice crystal growth in sugar solutions. *Int. J. Heat Mass Transf.* 2016, 95: 153-161.
- Van der Sman, R.G.M., Meinders, M.B.J. Analysis of improved Lattice Boltzmann phase field method for soluble surfactants. *Comput. Phys. Commun.* 2016, 199: 12-21.
- Van der Sman, R.G.M., Van der Graaf, S. Diffuse interface model of surfactant adsorption onto flat and droplet interfaces. *Rheol. Acta* 2006, 46(1): 3-11.
- Wang, H., Yuan, X., Liang, H., et al. A brief review of the phase-field-based lattice Boltzmann method for multiphase flows. *Capillarity* 2019, 2(3): 33-52.
- Wang, X., Kou, J., Cai, J. Stabilized energy factorization Approach for Allen-Cahn Equation with Logarithmic Flory-Huggins potential. *J. Sci. Comput.* 2020, 82(2): 25.
- Xu, J., Li, Z., Lowengrub, J., et al. A level-set method for interfacial flows with surfactant. *J. Comput. Phys.* 2006, 212(2): 590-616.

- Xu, J., Yang, Y., Lowengrub, J. A level-set continuum method for two-phase flows with insoluble surfactant. *J. Comput. Phys.* 2012, 231(17): 5897-5909.
- Xu, X., Di, Y., Yu, H. Sharp-interface limits of a phase-field model with a generalized Navier slip boundary condition for moving contact lines. *J. Fluid Mech.* 2018, 849: 805-833.
- Yan, X., Huang, Z., Yao, J., et al. Numerical simulation of hydro-mechanical coupling in fractured vuggy porous media using the equivalent continuum model and embedded discrete fracture model. *Adv. Water Resour.* 2019, 126: 137-154.
- Yang, Q., Yao, J., Huang, Z., et al. A comprehensive SPH model for three-dimensional multiphase interface simulation. *Comput. Fluids* 2019, 187: 98-106.
- Yang, X. Numerical approximations for the Cahn-Hilliard phase field model of the binary fluid-surfactant system. *J. Sci. Comput.* 2018, 74(3): 1533-1553.
- Yang, X., Ju, L. Linear and unconditionally energy stable schemes for the binary fluids surfactant phase field model. *Comput. Methods Appl. Mech. Eng.* 2017, 318: 1005-1029.
- Yuan, Z., Wu, R., Wu, X. Numerical simulations of multi-hop jumping on superhydrophobic surfaces. *Int. J. Heat Mass Transf.* 2019, 135: 345-353.
- Yue, P., Feng, J.J., Liu, C., et al. A diffuse-interface method for simulating two-phase flows of complex fluids. *J. Fluid Mech.* 2004, 515: 293-317.
- Zeng, Q., Yao, J., Shao, J. Study of hydraulic fracturing in an anisotropic poroelastic medium via a hybrid EDFM-XFEM approach. *Comput. Geotech.* 2019, 105: 51-68.
- Zhang, L., Jing, W., Yang, Y., et al. The investigation of permeability calculation using digital core simulation technology. *Energies* 2019, 12(17): 3273.
- Zhu, G., Chen, H., Yao, J., et al. Efficient energy-stable schemes for the hydrodynamics coupled phase-field model. *Appl. Math. Model.* 2019a, 70: 82-108.
- Zhu, G., Kou, J., Sun, S., et al. Decoupled, energy stable schemes for a phase-field surfactant model. *Comput. Phys. Commun.* 2018, 233: 67-77.
- Zhu, G., Kou, J., Sun, S., et al. Numerical approximation of a phase-field surfactant model with fluid flow. *J. Sci. Comput.* 2019b, 80(1): 223-247.
- Zhu, G., Kou, J., Yao, B., et al. Thermodynamically consistent modelling of two-phase flows with moving contact line and soluble surfactants. *J. Fluid Mech.* 2019c, 879: 327-359.
- Zhu, G., Kou, J., Yao, J., et al. A phase-field moving contact line model with soluble surfactants, *J. Comput. Phys.* 2020, 405: 109170.
- Zhu, G., Yao, J., Li, A., et al. Pore-scale investigation of carbon dioxide-enhanced oil recovery. *Energy Fuels* 2017, 31(5): 5324-5332.